NASS
NAN YANG ACADEMY OF SCIENCES

Sustainable Marine Structures
https://ojs.nassg.org/index.php/sms

ARTICLE

Dynamic Analysis of Splash-zone Crossing Operation for a Subsea Template

Adham M. Amer[1] Lin Li[1*] Xinying Zhu[2]

1. Department of Mechanical and Structural Engineering and Materials Science, University of Stavanger, Norway
2. Havfram AS, Stavanger, Norway

ARTICLE INFO

Article history
Received: 13 July 2022
Revised: 16 August 2022
Accepted: 31 August 2022
Published Online: 30 September 2022

Keywords:
Splash-zone crossing
Subsea template installation
Shielding effect
Allowable sea states

ABSTRACT

Subsea templates are steel structures used to support subsea well components. Normally, offshore crane vessels are employed to install them to the target location on the seabed. Crossing the splash-zone during the lowering of a subsea template is considered the most critical phase during the installation due to slamming loads and needs to be studied to provide the operational weather criterion during the planning phase. In this study, dynamic response analysis has been carried out to evaluate the allowable sea states for the plash-zone crossing phase of the subsea templates. The numerical model of the lifting system, including the crane vessel and the subsea template, is firstly built in the state-of-the-art numerical program SIMA-SIMO. Then, dynamic analysis with time-domain simulations is carried out for the lifting system under various sea states. The disturbed wave field due to the shielding effects from the installation vessel is considered when calculating the hydrodynamic forces on the template. Statistical modelling of the dynamic responses from different wave realizations is used to estimate the extreme responses of various sea states. The application of the generalized extreme value distribution and Gumbel distribution in fitting the extreme responses is discussed. Moreover, the influence of the shielding effects from the vessel, as well as the influence of the changing size of the suction anchor on the hydrodynamic responses and the allowable sea states are studied.

1. Introduction

The lowering operation of subsea assets through the wave splash-zone is considered the critical phase during an offshore installation process. The combined high costs and sensitivity of the operation to weather conditions reduce the possibilities to correct errors during the installation process. The consequence of the failure of the operation is significant. Thus, numerical modelling of the installation system is required during the planning phase to tackle both the uncertainties and high risks involved in such operations. Various numerical studies have been performed to analyze the dynamic responses of lifting operations when the lifted objects cross the splash-zone. These stud-

*Corresponding Author:
Lin Li,
Department of Mechanical and Structural Engineering and Materials Science, University of Stavanger, Norway;
Email: lin.li@uis.no

DOI: http://dx.doi.org/10.36956/sms.v4i2.596

ies addressed the dynamic responses during the installation of different subsea assets such as subsea trees [1], manifolds [2,3], templates [4], suction anchors [5], and spools [6]. In a typical offshore lowering operation, the vessel hull is used to shield the lowered asset from the incident waves. The hull diffracts the incoming waves and reduces the overall dynamic forces acting on the subsea asset as the lowering takes place. This phenomenon is known as shielding effect. Developing an adequate numerical model to account for shielding effect requires an accurate calculation of the diffracted wave data around the installation vessel. Several studies proposed numerical approaches to consider the shielding effect from the installation vessel while lowering subsea assets, such as monopiles and spools, through splash-zone [6,7].

Performing time-domain simulations for the lowering system is a common approach to carry out such numerical studies. The numerical modelling requires a proper estimation of the hydrodynamic loads acting on the marine structure. Generally, this needs an accurate estimation of both added mass and damping coefficients of the submerged structural members [8,9]. The estimation of these coefficients is quite challenging, especially when perforated elements such as suction anchors are considered.

Lifting operations within a limited duration are often classified as weather-restricted operations. For such operations, it is required to establish the operational limits during the planning phases. For marine lifting operations sensitive to wave loads, these limits are often given as functions of significant wave height (Hs), spectral peak period (Tp), wave direction, etc. In similar studies, operational limits are obtained through numerical simulations, model tests, field measurements, offshore observations, or a combination of what previously mentioned [10]. Among them, numerical simulations are less expensive and are mostly applied to study the critical responses during operations and compare the dynamic responses with the operational criteria to provide the operational limits [11].

This study focuses on the lifting operation of a subsea template. Subsea templates are used to provide guidance and support for well drilling equipment and other completion activity taking place on the seabed. They also act as supporting frames for other subsea production system components, including manifolds, risers, and wellheads. Subsea templates are normally installed by a floating crane vessel at a deep offshore site [12]. The installation process of subsea templates consists of different phases. First, the template is over-boarded by the installation vessel. After being lifted-off from the deck of the installation vessel, the template is lowered through the wave splash-zone. Finally, the template is further submerged until it reaches the seabed. A typical subsea template usually has four suction anchors. Due to the large cross-sectional area of the anchors, the template experiences high hydrodynamic loads when crossing the splash-zone. Furthermore, the dynamic features of such operations undergo continuous changes and are dominated by non-linear responses. Thus, the prediction of the motion responses and the estimation of the slamming loads on the subsea template in the wave zone can be quite challenging. Several numerical studies were conducted to capture the dynamic responses when lowering subsea structures through the splash-zone [1,2,5,6, 13-16].

According to DNV standards, several operational criteria shall be considered during the splash-zone crossing phase of the lifting operation [9]. The first criterion is to evaluate the potential for damage to the lowered object due to the slamming loads. The other criterion is on the potential for snapping forces acting on the lift wire and slings due to the slack limit being reached. Here, the snap force is defined as a dynamic force within a short duration, which is associated with any sudden changes within the lifted object velocity [17].

This paper presents a numerical study on the splash-zone crossing operation for a subsea template. The installation system and the numerical model used in this study are firstly introduced. Then, a validation of the numerical results with actual field measurements is performed. Next, the operation acceptance criteria and the statistical models used to assess the allowable sea states are given, followed by time-domain and eigen value analysis of the numerical model. Lastly, the dynamic responses and the allowable sea states for different sensitivity studies are presented with detailed discussions.

2. The Installation System and the Numerical Model

The lifting system consists of two main bodies the installation vessel and the subsea template. A typical offshore installation vessel is used for the operation [6], and the vessel technical specifications are presented in Table 1.

Table 1. Installation vessel technical specifications.

Item	Unit	Value
Overall length	[m]	156.7
Overall breadth	[m]	27
Displacement at maximum draft	[ton]	1.70E4
Maximum draft	[m]	8.5
Crane maximum lift capacity	[ton]	400
Crane operating radius	[m]	10 - 40

A typical integrated template structure (ITS) is applied in the numerical model [18], and the side and top views of the template can be found in Figure 1. The template structure mainly consists of four hollow suction anchors, four hollow washout sleeves, and eight guideposts attached to the top of the template. The overall length and width of the subsea template are 20.8 m and 17.4 m, respectively, and the overall height from the top of the guideposts to the bottom of the anchors is 12.9 m. The total mass of the template is 263 tons. The mass of the template is distributed evenly at the four corners, making an easy four-sling arrangement for handling the template in the air and during the lowering operation into the water. The dimensions of the main elements of the template are presented in Table 2.

Table 2. Subsea template dimensions and specifications.

Item	Unit	Value
Overall height	[m]	12.9
Overall length	[m]	20.8
Overall width	[m]	17.4
Mass in air	[ton]	263
Outer diameter of the suction anchors	[m]	5.5
Outer diameter of the washout sleeves	[m]	0.98
Wall thickness (suction anchors and washout sleeves)	[m]	0.02
Height of the suction anchors height	[m]	8.225
Height of the washout sleeves	[m]	7.725
Carbon steel density	[kg/m^3]	7850

The crane, crane lift wire, slings, and winch compose the hoisting system for the lifting operation of the template. Because of the large dimension of the template structure, four slings on top of the four suction anchors are applied to distribute the tension in the slings. The four slings connect the template to the hook of the crane block, and the lift wire connects the crane block and the crane tip. The slings maintain a fixed length during the installation process, while the main lifting wire increases in length as lowering takes place. The winch speed is normally kept at a low value during splash-zone crossing. For this study, the lowering speed of the winch is kept at 0.1 m/s.

2.1 Numerical Model

The numerical model has been built using the marine operation numerical program SIMA-SIMO [19]. The coupled numerical model consists of the installation vessel, the template, and the hook. Both the installation vessel and the template have six degrees of freedom (DOFs), and the hook only has three DOFs. The global coordinate system is highlighted in Figure 2. The origin is located at the free water surface, and the middle section of the installation vessel. The X-axis points towards the bow of the vessel, the Y-axis points towards the port side, and the Z-axis points upwards. The crane's operating radius is set to 18m during the operation. The established numerical model of the operating system is shown in Figure 2.

The wire couplings through four slings and the lift wire are modeled as linear springs. The axial stiffness, k can be expressed as:

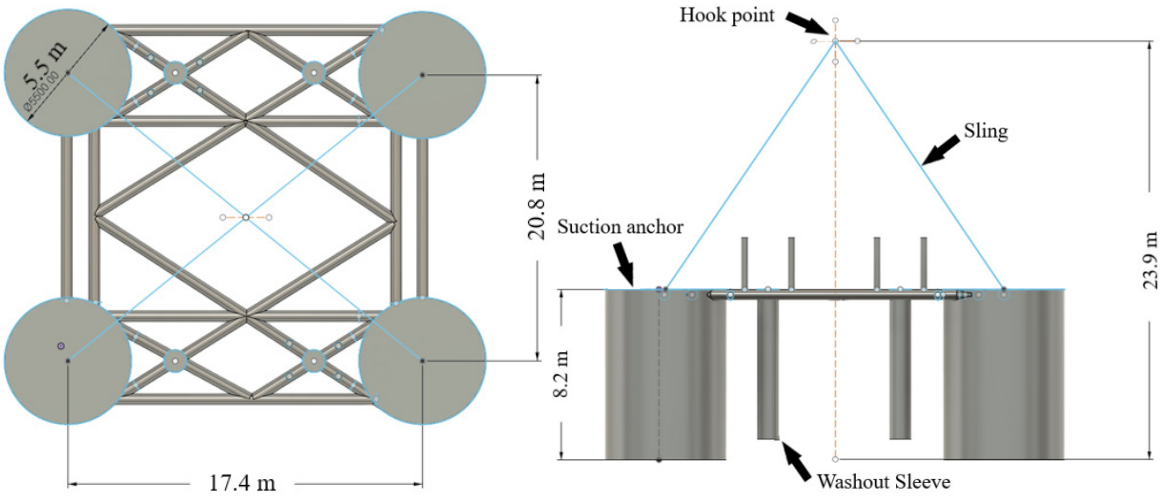

Figure 1. Top and side views of the subsea template used in the numerical model.

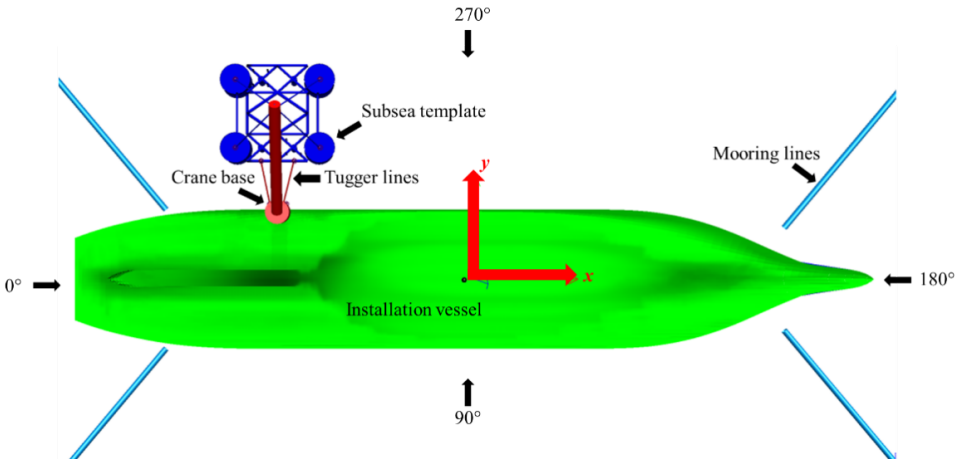

Figure 2. Coupled numerical model in SIMA-SIMA.

$$\frac{1}{k} = \frac{l}{EA} + \frac{1}{k_o} \quad (1)$$

where EA is the modulus of elasticity times the cross-sectional area of the wire; l is the effective length of the wire, and it changes for the main lift wire when the winch runs during the lowering operation. $1/k_o$ is the connection flexibility. The properties of the wires are chosen based on the practical operations, and they are given in Table 3.

Table 3. Properties for the lift wire and slings.

Item	Unit	Lifting Wire	Slings
Unstretched length	[m]	39.8	18.1
Connection flexibility	[m/N]	1.3e-07	1.3e-07
Damping	[Ns/m]	1.0e+07	6.16e+06
Axial stiffness EA	[N]	1.2e+09	3.08e+08
Breaking strength	[N]	1.3e+07	6.1e+06

Tugger lines are usually used in lowering operations to control the yaw motion of the template. In this study, a constant tension is applied to two crane tugger lines. Both lines are connected to the template structure and the crane base (see Figure 2). To illustrate the function of the tugger lines, the yaw motion of the template during the lowering phase with and without the two crane tugger lines is compared and shown in Figure 3 under the same sea state. A large increase in the template yaw angle from 0 to 140 degrees can be clearly observed without using any tugger lines. This large yaw is undesirable and should be avoided for a safe operation. By adding two tugger lines with 5 ton's tension in each line, the mean yaw angle of the template maintains around 0 deg, and less fluctuation in the yaw motion is seen after 300 s after the template crosses the splash zone. Thus, the tugger lines are important in the numerical model to avoid large yaw motion for the template during the whole lowering process.

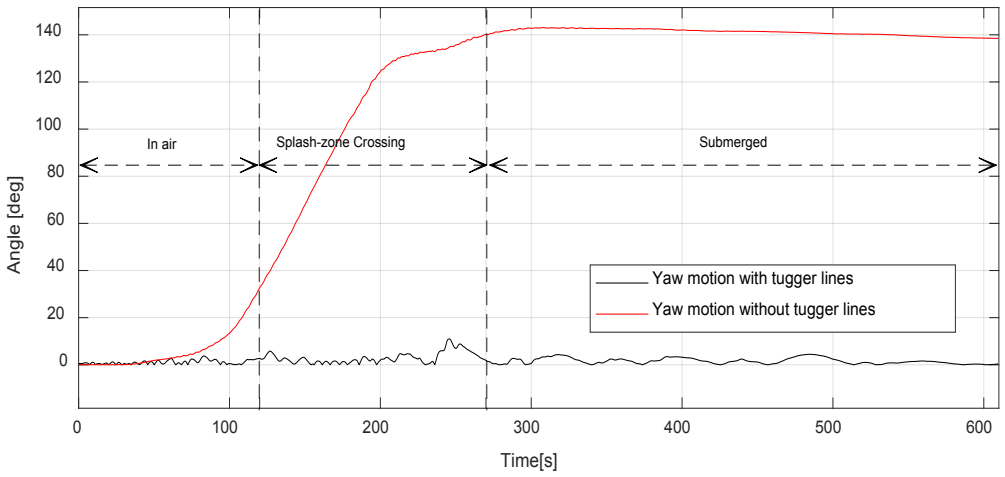

Figure 3. Template yaw motion at Hs = 2 m and Tp = 8 s.

Modeling of hydrodynamic forces on the template

The template is modeled in SIMA-SIMO using slender elements. The empirical Morison's formula is considered suitable to calculate hydrodynamic forces for slender elements with a D/L ratio (diameter over wavelength) much less than 0.2 [20]. Each slender element is divided into several strips. Based on Morison's equation, the wave force per unit length on each strip normal to the member, F_s, is given as follows:

$$F_s = \rho_w(1 + C_A)\frac{\pi D^2}{4}\ddot{\zeta}_s - \rho_w C_A \frac{\pi D^2}{4}\ddot{x}_s + \frac{1}{2}\rho_w C_q D|\dot{\zeta}_s - \dot{x}_s|.(\dot{\zeta}_s - \dot{x}_s) \quad (2)$$

where ρ_w is the fluid density; D is the outer diameter of the element; and C_A and C_q are the added mass and quadratic drag force coefficients, respectively. $\ddot{\zeta}_s$, $\dot{\zeta}_s$, $\ddot{x}_s$ and $\dot{x}_s$ are accelerations and velocities of the fluid and the element itself, respectively.

The reference volume when calculating the vertical added mass of one such anchor equals the volume of the entrapped water inside the cylinder plus the volume of a sphere with a radius equal to the radius of the anchor. This reference volume is illustrated in Figure 4. For the top hatches of the suction anchors, they are normally open in the actual operations, and thus a perforation effect for each suction anchor takes place. For the subsea template used in this study, a perforation percentage of 6% is accounted for each anchor. This percentage causes a reduction in the value of the vertical added mass according to the following expression [8],

$$A_{33} = A_{33o}\left(0.7 + 0.3\cos\left[\frac{\pi(p-5)}{34}\right]\right) \quad (3)$$

where A_{33} is the perforated vertical added mass, A_{33o} is the non-perforated vertical added mass, and p is the perforation ratio in percentage. If p is less than or equal to 5%, the vertical added mass is assumed to be non-perforated and A_{33} will be equal to A_{33o} in the previous formula.

The experimental study performed by Solaas and Sandvik (2017) is used to calculate the damping of the suction anchor in the axial direction [21]. Free oscillation decay tests in the axial direction were performed for anchors with different height to diameter ratios and perforations to provide an accurate measurement of the hydrodynamic coefficients. These experiments concluded that for anchors with a perforation ratio of over 4%, the axial linear damping term is primary, and the quadratic damping term is secondary. Since the anchor used in this study has a perforation of 6%, only linear damping in the axial direction needs to be considered. Figure 5 includes the linear damping data of an anchor having a diameter of 5 m and a height of 8.9 m. By scaling the linear damping with the introduced anchor diameter in Table 2, the new vertical damping value can be estimated. The horizontal damping for each anchor is estimated according to DNVGL-RP-N103 recommended practice [8].

Three slender elements, namely the vertical, top, and bottom elements, are employed in SIMA-SIMO to distribute the hydrodynamic forces acting on each anchor. The inputs of each of these elements are presented in Table 4. The inputs are assigned in the elements local coordinate system in SIMO.

The vertical element, which has the same height as the anchor, is modeled to consider numerical properties including the structural mass, volume, lateral added mass, and damping. The lateral added mass (Ma_{La}) for the vertical element is set to be equal to the added mass of a cylinder normal to the flow plus the mass of the entrapped water inside the anchor (see Figure 4).

The element located at the top of the anchor is used to model the added mass caused by the water above the anchor roof and the damping due to the flow through the ventilation hatches at the top. Ma_{Ax} for the top element equals the perforated vertical added mass of the upper half of the water sphere divided by the element length (see Figure 4). The total perforated added mass is calculated from Equation (3). The quadratic drag components (D_{2La}) for the top and vertical elements are calculated based on the given guidelines in DNVGL-RP-N103 [8].

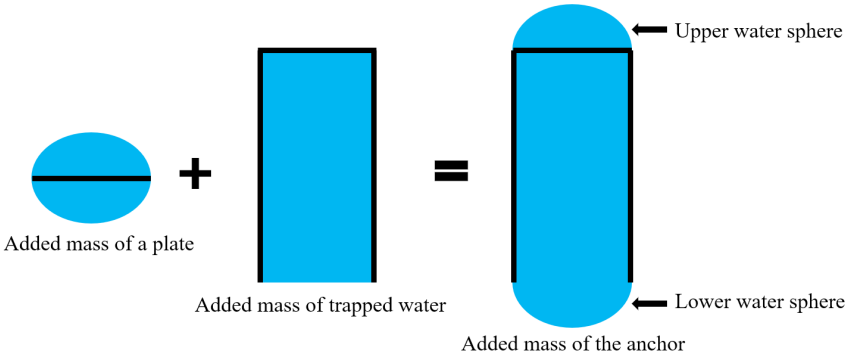

Figure 4. Illustration of the reference volume for the added mass of a suction anchor in the vertical direction.

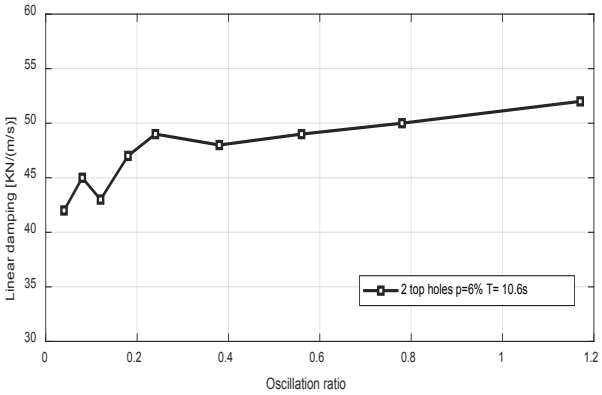

Figure 5. Axial linear damping of a suction anchor with two top holes and 6% perforation ration [21].

Table 4. Slender elements hydrodynamic coefficients input in SIMO.

			Vertical element	Top element	Bottom element
Item	Description	Unit	Value	Value	Value
D_{2Ax}	Axial quadratic damping	Ns^2/m^3	-	-	-
D_{2La}	Lateral quadratic damping	Ns^2/m^3	5800	5800	-
D_{1Ax}	Axial linear damping	Ns/m^2	-	-	5.7e+05
Ma_{Ax}	Axial added mass	kg/m	-	2.32e+05	2.42e+06
Ma_{La}	Lateral added mass	kg/m	39910	39910	-

Another element in the numerical model located at the bottom of the anchor accounts for the hydrodynamic properties that generate slamming forces. The element is located at the bottom tip of the anchor to use the wave kinematics at the entrance of the anchor when calculating the slamming forces during time-domain simulations. Ma_{Ax} for the bottom element is the sum of the perforated vertical mass of the trapped water and the lower half of the water sphere divided by the element length. The element has a length of 0.1 m. The axial linear drag D_{1Ax} for the bottom element is estimated based on linear damping data presented in Figure 5. Depth-dependent coefficients (DDC) are used to ensure that the forces appear when the suction anchor roof touches the instantaneous water surface. The DDC used in this model are defined in Figure 6 and Table 5. RMa_{Ax} and RD_{1Ax} are the ratios of relative axial added mass and relative axial linear drag, respectively. Both terms are assigned in SIMO to control the development of both axial drag and added mass as the template gets submerged. The value is assigned between 0, which means that the hydrodynamic term is not yet developed, and 1 which means the hydrodynamic term is fully developed. Since the added mass is at its highest only when the roof of the anchor reaches the wave surface, RMa_{Ax} is set to 0 along the anchor length (position A to C). Once the anchor roof reaches the free water surface (position D to E), the added mass starts developing from 0.9 to 1. As for RD_{1Ax}, a slight development of damping takes place when the bottom of the anchor touches the water surface (position B to C). Same as the added mass, the damping becomes fully developed from 0.8 to 1 when the anchor roof reaches the water surface (position D to E).

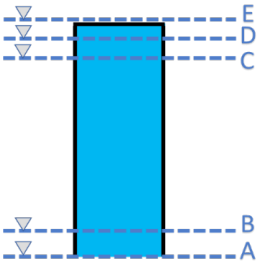

Figure 6. Depth-dependent coefficients activation levels for each anchor.

The total hydrodynamic calculations of the template, including the top structure, are presented in Table 6. The table clearly shows that most of the inertia forces are caused by the template total added mass. The total added mass in both axial and lateral directions is almost 5 times larger than the actual mass of the template. This significantly large added mass value may generate large slamming loads on the subsea template model when it crosses the splash-zone according to Equation (2).

Table 5. Depth-dependent coefficients inputs in SIMO

Position	Description	Anchor slender element vertical location in global coordinate [m]	RD_{1Ax}	RMa_{Ax}
A	anchor above water level	0	0	0
B	anchor penetrates water level	–0.1	0.1	0
C	anchor roof above water level	–8.025	0.1	0
D	anchor roof partially submerged	–8.125	0.8	0.9
E	anchor roof completely submerged	–8.225	1.0	1.0

Table 6. Total hydrodynamic calculation of the template

Item	Unit	Value
D_{2Ax}	kNs^2/m^2	64
D_{2La}	kNs^2/m^2	290
D_{1Ax}	kNs/m	57
Ma_{Ax}	ton	1152
Ma_{La}	ton	1381

2.2 Environmental Conditions

Disturbed wave kinematics

The wave field close to the vessel is different from incident waves when the construction vessel is present, and this disturbance of the wave field is known as "shielding effects". Because of this, the hydrodynamic forces on the subsea template are affected when it crosses the wave zone. To take into account the influence of the disturbed wave fields during the lowering operation, a numerical method was developed by interpolating the disturbed wave kinematics in both horizontal and vertical directions at each instance when calculating the hydrodynamic forces of a monopile during the lowering operation [22,23]. The same method was applied to the spool lowering operation [6], but the disturbed wave kinematics were only interpolated in the horizontal plane at the mean free surface since spools mainly consider horizontal elements. In the vertical direction, a decay formula as in incident waves for the wave kinematics was used. Although subsea templates contain both horizontal and vertical elements, the critical loads during lowering occur when the top roof of the anchors touches the water surface. When the anchor roof crosses the splash-zone, the added mass component theoretically increases from zero and becomes fully developed over a short vertical distance [24]. Thus, the decay formula in the vertical direction is also applied in this study for simplification.

Numerical program WADAM is applied to calculate the RAOs for the disturbed wave kinematics caused by the vessel diffraction and radiation using potential flow theory [6]. Figure 7 shows the contour of the RAOs of the disturbed wave elevation near the installation vessel with a 165 deg wave direction (long-crested waves) as an example. The initial positions of the subsea template anchors are highlighted in the figure. When the wave period is 12 s, the disturbed wave kinematic RAOs are close to those from the incident wave with RAO values close to 1. However, as the waves become shorter with 6 s peak period, the RAOs are greatly reduced due to the shielding effects. Moreover, it is also observed that the shielding effect is stronger when the location is closer to the stern under shorter wave conditions at a given wave direction.

Short-crested waves and shielding effect

In real sea conditions, the wind-generated seas are often short crested with wave energy spreading in different directions. This spreading of wave energy may cause different forces and motions than those under long-crested waves. In this study, short-crested waves with different combinations of Hs and Tp are used in the numerical simulations. For each combination of Hs and Tp, JONSWAP spectrum is used to generate random waves. The spectrum considering the short-crestedness of the waves is then formulated by the JONSWAP wave spectrum S(ω) and the directional spreading function D(θ) :

$$S(\omega,\theta) = S(\omega)D(\theta) \tag{4}$$

$$D(\theta) = \begin{cases} C(n)cos^n(\theta-\theta_0) & |\theta-\theta_0| \le \pi/2 \\ 0 & |\theta-\theta_0| > \pi/2 \end{cases} \tag{5}$$

$$C(n) = \frac{1}{\sqrt{\pi}} \frac{\Gamma(1+n/2)}{\Gamma(1/2+n/2)} \tag{6}$$

where θ_0 is the main wave direction. The spreading index n describes the degree of wave short-crestedness, and n $\rightarrow\infty$ represents a long-crested wave field. Offshore lifting operations are usually carried out in relatively low sea states. Thus, the wave spreading is more significant when compared to higher sea states. In this study, a constant n = 2 is used in the spreading function when generating short-crested waves, and this index is considered reasonable to represent wind-generated seas in relatively low waves. Furthermore, the disturbed wave field caused by

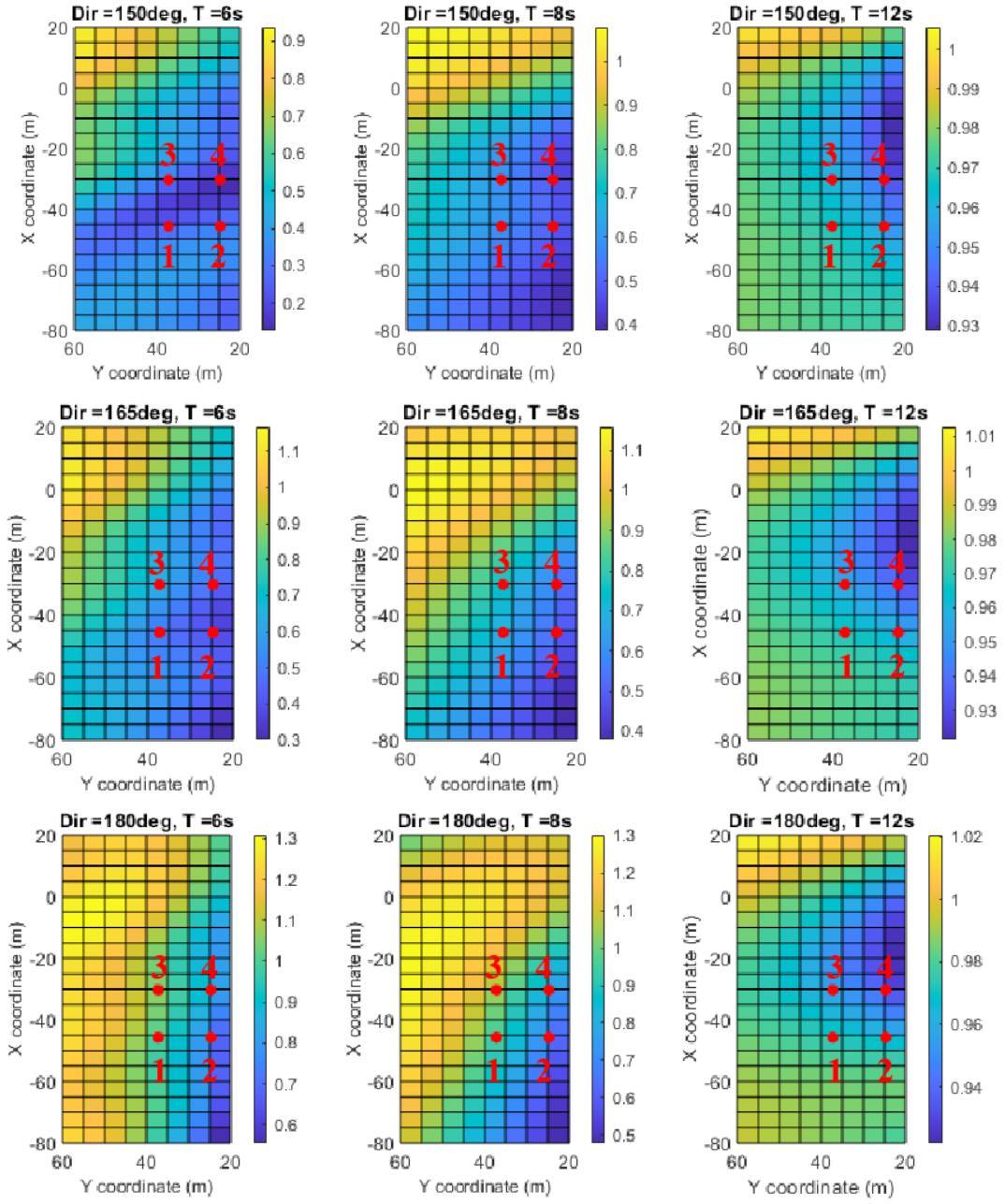

Figure 7. RAOs of the wave elevation in disturbed wave region near the installation vessel at three different directions.

the shielding effects is highly influenced by the wave direction, as shown in Figure 7. Thus, the effects of short-crested waves and the shielding must be accounted for at the same time in the numerical analysis when calculating the responses of the lifting system.

3. Operational Criteria and Statistical Models

3.1 Operational Criteria

Based on DNV guidelines for lifting operations [8,25], two main criteria for the splash-zone crossing, i.e., the maximum load on the main lift wire and the slack of the main lift wire and slings, are considered when assessing the allowable sea states.

For offshore lifting operations, the recommended dynamic amplification factor (DAF) for a static hook load (SHL) between 100 tons and 300 tons is 1.25. For the studied case, the SHL is around 275 tons, so the maximum allowable dynamic hook load (DHL) is calculated as 345 tons. By checking the lifting capacity of the crane equipment, this DHL value is within the operational capacity of the vessel's crane. Furthermore, the crane itself

requires a maximum value of DAF shall not exceed 1.3, with a maximum static load of 320 tons when the working radius of the crane is 18 m. Based on this requirement, the maximum dynamic tension of the crane lift wire should not exceed 416 tons during the whole operation.

Regarding the slack sling criterion, the DNV standards require a minimum margin against slack which is 10% of the minimum static weight and therefore 10% of the static load for the hoist line and slings, respectively. If some components are hollow and subjected to flooding during submergence, the submerged weight should be taken as the minimum static weight without considering flooding. For the current study, the submerged weight of the subsea template is 230 tons. Therefore, based on the required 10% margin against the slack criterion, the minimum dynamic tension in the main lift wire should not be less than 23 tons, and for each sling, the dynamic tension should never be less than 6 tons during the whole lowering operation.

The above two criteria are used to assess the allowable sea states for the splash zone crossing operation of the subsea template.

3.2 Statistical Models

Because of the variability of stochastic waves, statistical modeling of the critical extreme responses is used during the assessment of the allowable sea states. In this study, the critical responses include the maximum and minimum tensions in the main lift wire and slings during the splash-zone crossing. The maximum (or minimum) tensions from all wave seeds are fitted into a selected statistical model, and the extreme values can be obtained from the fitted statistical model. The sensitivity of the obtained extreme responses depends on the probability of non-exceedance. In practice, a value between 0.9 and 0.99 is chosen according to the associated risks of the operation. In this study, the assigned target probability of non-exceedance is 0.95.

Gumbel extreme value distribution is widely used in predicting both maximum and minimum extreme responses for different offshore structures [26]. The cumulative distribution function (CDF) of Gumbel distribution of a random variable X is given by

$$F_x(x;\lambda,\kappa) = exp\left[-\exp\left(\frac{x-\lambda}{\kappa}\right)\right] \quad (7)$$

where λ and κ are the location and scale parameters of the distribution, respectively.

This study investigates the possibility of achieving a better statistical representation of the operation's extreme responses by comparing Gumbel and Generalized Extreme Value Distribution (GEV) fittings. When dealing with a small number of available data, a two-parameter fitting can be quite poor due to the lack of flexibility. To overcome this, generalizations of the Gumbel distribution were introduced. GEV combines Gumbel, Fréchet, and Weibull extreme value distributions, which provides more flexibility in fitting a population of data compared to Gumbel. The CDF of the GEV distribution is given by

$$F_x(x;\lambda,\kappa,\beta) = \exp\left(-\left[1+\beta\left(\frac{x-\lambda}{\kappa}\right)\right]^{-\frac{1}{\beta}}\right) \quad (8)$$

where λ, k, β are the location, scale, and shape parameters of the distribution. The maximum and minimum values for the lift wire and slings are extracted from the response time series for each sea state realization (seed). Then, the parameters of both Gumbel and GEV distributions are estimated using the maximum likelihood method by fitting the responses from all wave seeds. The extreme values are then obtained from the fitted distribution at the given probability of non-exceedance.

4. Model Validation with Field Measurements

Before the allowable sea state assessment is carried out, a validation of the numerical model and numerical results is performed to ensure that the employed numerical model is accurate enough. The validation is to compare the numerical results with the crane logging time history from the same installation vessel during the actual offshore deployment. The logging data are from the installation of a template with a similar footprint to the one used in this study. However, the total weight of the installed template is smaller than the one used in the model. Thus, the current template model is modified in SIMA-SIMO to match that of the installed one. Because the exact wave elevation data were not recorded during the field measurement, various realizations of the waves (seeds) are used for the same Hs and Tp condition in the numerical simulations to validate the results. The effect of variability in seed numbers is further discussed in section 6.3.

Figure 8 compares the lift wire tension of both field measurements and SIMO model. The top plate of the subsea template enters the free surface at approximately 240 s. It is shown that the estimation of the slamming forces at 240 s agrees well with the field measurements. The fluctuations in the lift wire tension from the numerical model matched those from the logged data, especially for seed no.10. The maximum and minimum tension values from SIMO do not show any significant deviation from the measured data in the first 300 s. In seed no.27, the tension force is slightly overestimated after 300 s, while in seed no.10, the force in the lift wire is slightly underestimated for the same time segment. This slight deviation does not

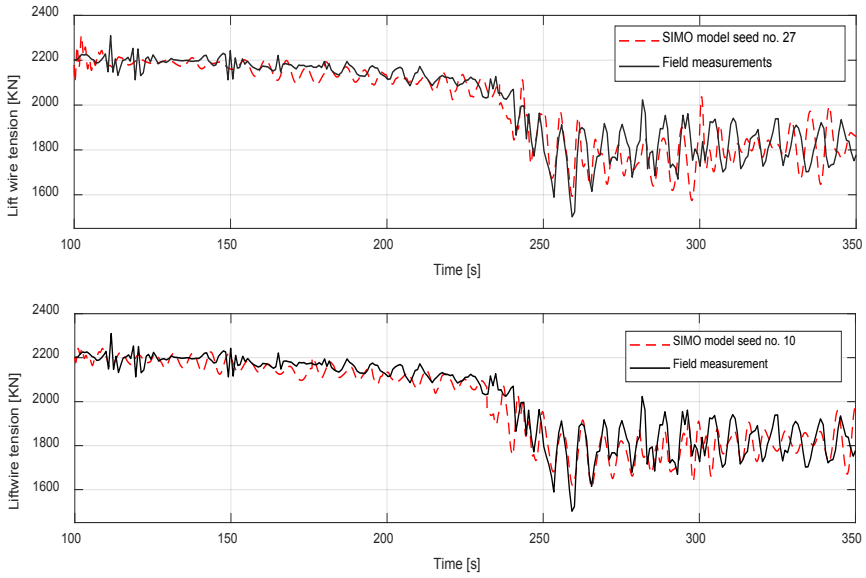

Figure 8. Comparing lift wire tension field measurements with SIMO model (Hs=1.9 m, Tp=6 s) with shielding effect.

impose any limitation on using the established numerical model in this study. Due to the stochastic nature of waves, it is very challenging to capture all variations of the tensions due to lack of exact wave elevation information. However, this comparison validates that the current model is capable to provide accurate estimation of the maximum and minimum tensions in the splash zone crossing process.

5. Eigenvalues and Time-domain Analysis

5.1 Eigenvalues Analysis

The natural periods of the system are obtained from the eigenvalue analysis. The analysis is conducted without including any external forces or damping effect and the following equation of motion is solved in the frequency domain:

$$[-\omega^2(\boldsymbol{M}+\boldsymbol{M}_a)+\boldsymbol{K}]\cdot\boldsymbol{x}=0 \quad (9)$$

where, ω is the natural frequency; $\boldsymbol{M}$ and $\boldsymbol{M}_a$ are the mass and added mass matrices of the system; $\boldsymbol{K}$ is the stiffness matrix, and $\boldsymbol{x}$ is the motion vector. The mass matrix includes both structural and hydrodynamic added mass. The analysis is performed for three different vertical locations for the template prior to the evaluation of the time-domain simulation results. These locations are illustrated in Figure 9 and defined when:

a) The anchor bottom is just above the free water surface

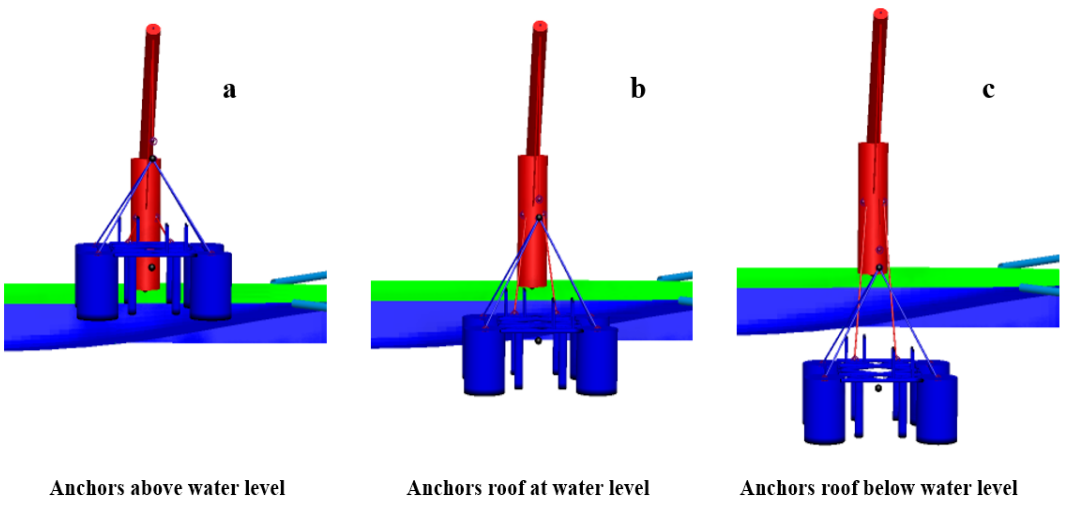

Figure 9. Template vertical positions in SIMO for frequency domain analysis.

b) The anchor roof is at the free water surface
c) The template is fully submerged

Table 7. Coupled system natural periods at three vertical positions of the template. (The vertical positions of the anchor roof relative to the mean free surface are used)

z = 8 m	z = 0 m	z = –8 m	Dominant motions
3.56 s	3.86 s	3.77 s	Template heave & vessel roll
6.91 s	6.94 s	6.96 s	Vessel roll & pitch
8.01 s	8.03 s	8.04 s	Vessel roll & heave
8.86 s	-	-	Template pitch & surge
14.28 s	-	-	Template roll & sway

To simplify the static analysis, the three degrees of freedom (DOF) of the hook are neglected when obtaining the natural periods of the installation system. Thus, the coupled system has 12 DOFs corresponds to 12 modes in total. The most critical position of the template is obtained from the transient dynamic responses in the time-domain simulations. This position is defined when the anchor roof crosses the splash zone. The natural periods of the coupled system are presented in Table 7. At short periods, the system is mainly dominated by the template heave and vessel roll motion for all given template positions. As the natural periods start approaching 8 s, both the pitch and heave motions of the vessel share dominance with the roll motion over the coupled system. Furthermore, when the template is still in air (z=8 m), the template pendulum motion dominates the system at long periods. However, this dominance starts shifting out of the peak periods operational range when the anchors roof is at the free water surface (z=0 m) or deeply submerged (z= –8 m).

5.2 Time-domain Simulations

Both the transient and the steady-state approaches are applied in the time-domain simulations in this study. In both approaches, the equations of motion are solved by numerical integration with a time-step of 0.02 s. The wave excitation forces on the construction vessel are pre-generated from the transfer functions obtained from the frequency-domain analysis. The radiation effects on frequency-dependent added mass and damping forces are included in terms of coupled retardation functions in the time domain. The calculation of wave forces on the subsea template is based on the instantaneous locations of each slender element of the template. The tensions in the wires are directly calculated for each time step based on the relative motions between the bodies.

5.2.1 Transient Approach

In the transient approach, the winch starts at 100 s and stops at 600 s with a speed of 0.1 m/s. An example of the dynamic responses of the lift wire tension is presented in Figure 10. In air, the tension acting on the lift wire is mainly due to the template weight. The dynamic force acting on the lift wire starts to decrease gradually due to buoyancy from 130 s when the template anchors are entering the water. When the template is fully submerged at 290 s, the water fills at a steady rate of 144 kg/s for a period of 110 s.

As lowering takes place, a fluctuation in the lift wire tension takes place due to the vessel motion and the slamming loads caused by the wave kinematics. It is noticed that this fluctuation is more intense when the anchors roof reaches the free water surface around 260 s. The vertical position of the template is projected on the XY plane, and the tension time history is projected on the XZ plane in Figure 10. The figure clearly shows that the highest response occurs when the anchor roof is at the free water surface (the template vertical position is close 0 m in XY plane). When the template is fully submerged, the wave kinematics starts decaying exponentially, thus reducing the slamming loads on the template.

5.2.2 Steady State Approach

The steady state approach is performed by placing the template at the most critical submergence during the whole simulation duration with zero winch speed. As previously shown in Figure 10, the largest dynamic response of the lift wire tension occurs when the suction anchor roof reaches the free water surface. In the steady state method, the template is placed where the mean position of the anchor roof is at the mean water surface. The simulation length is set to the same as the duration of the transient approach. Figure 11 compares the lift wire tension using the transient and steady state approach. The hydrodynamic forces are more violent when using the steady state approach. Such outcome is expected since the anchor roofs are constantly subjected to the highest wave kinematics at the free water surface, which increases the tension forces on the lift wire according to Equation (2). However, the lift wire tension behavior starts to be similar between the two approaches after the anchor roof reaches splash-zone around 260 s in the transient case. At this time instance, the template starts experiencing the same dynamic loads due to wave kinematics at the free water surface. As the template is getting fully submerged, the intensity of the slamming loads in the transient case is less compared to the steady state due to the decaying effect.

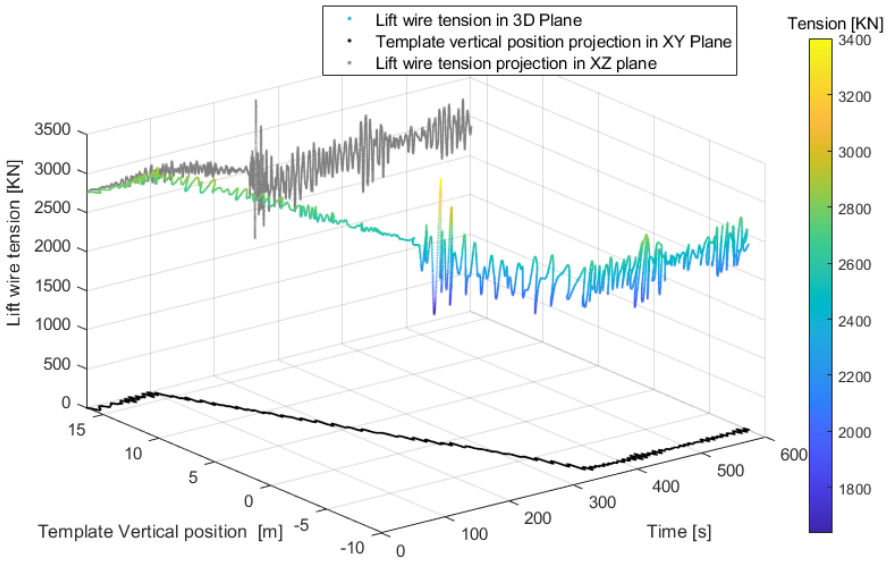

Figure 10. Lift wire tension using transient approach (Hs = 1.8 m, Tp = 8 s, and Dir = 165 deg), without shielding effect.

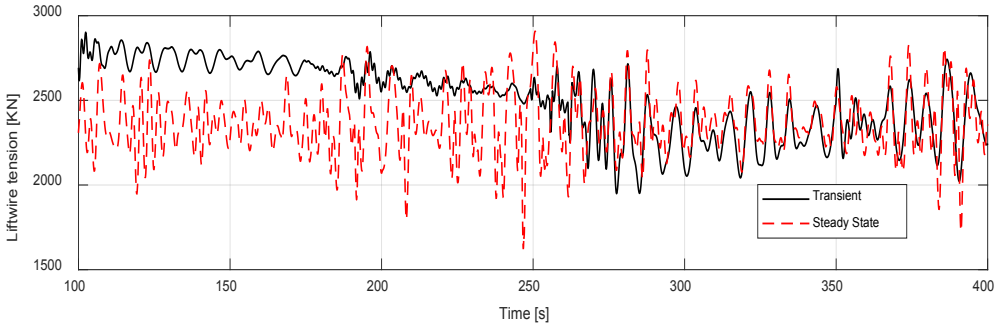

Figure 11. Comparison of responses using steady-state and transient analysis methods (Hs = 1.8 m, Tp = 8 s, and Dir = 165) without shielding effect.

6. Dynamic Responses and Allowable Sea States Assessment

6.1 Dynamic Responses with and without Shielding Effect

The lift wire dynamic responses indicate that the maximum tension criterion defined in Section 4 is more critical for the operation than the slack wire criterion. It is also noticed that the dynamic responses of the system during splash-zone crossing can differ greatly with different input sea realizations for the same sea state due to the stochastic nature of waves. Figure 12 provides a comparison of the lift wire tension at two different sea realizations with the same Tp and Hs. Seed no.29 clearly exceeds seed no.48 in terms of maximum and minimum tension. The figure also shows that the minimum slack criterion does not impose any limitation on the evaluated sea states. The wave elevations at the location where the center of the template is lowered into the water using the two wave seeds are also compared in Figure 12. The comparison shows that the maximum wave elevation when the anchor roof reaches the splash-zone (between 260 s and 265 s) is almost 0.15 m at seed no.48 and 1 m at seed no.29. Thus, higher slamming loads are expected at seed no.29 compared to seed no.48.

When the shielding effect is considered, a decrease in the lift wire tension is observed. Figure 13 compares the time history of the lift wire tension with and without shielding effect using the transient approach. For the results with shielding effect included, the dynamic forces are reduced when the suction anchor roof reaches the splash-zone (around 260 s) for Tp = 8 s. However, the influence of the shielding effect is almost absent at the higher peak period with Tp = 12 s, where the maximum

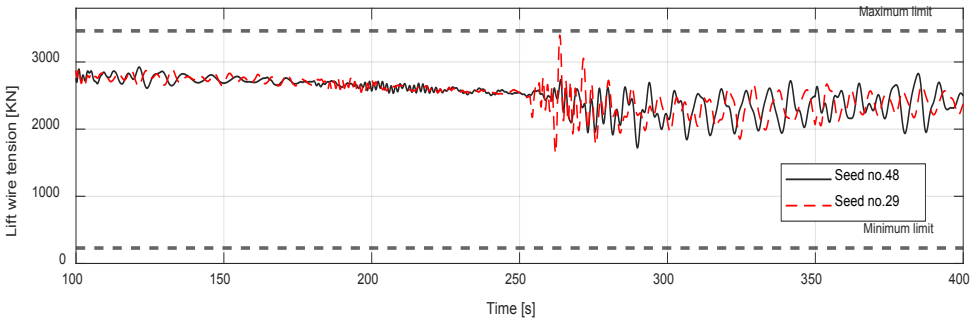

(a) Lift wire tension

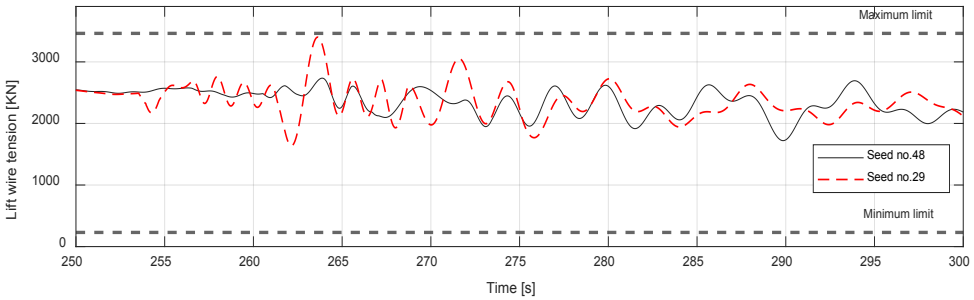

(b) Lift wire tension from 250s to 300s

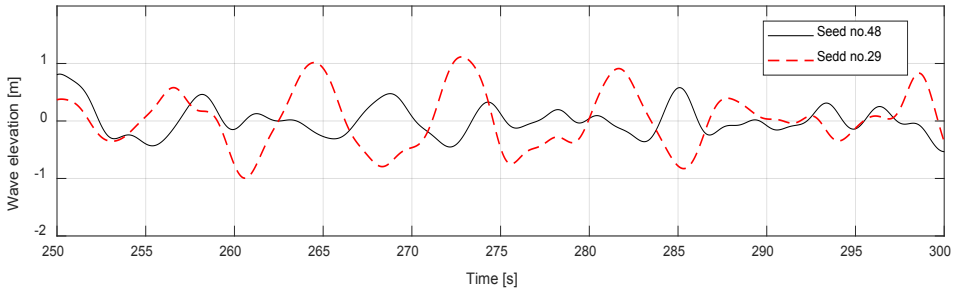

(c) Wave elevation from 250s to 300s

Figure 12. Time histories of lift wire tension and wave elevation of two different wave realizations for the same sea state (Hs=1.8 m, Tp=8 s, Dir=165 deg) without shielding effect.

lift wire tension is 2865 KN and 2832 KN with and without shielding, respectively. This outcome aligns with the obtained wave kinematic RAO in the disturbed waves region near the template in Figure 7. The RAO of the wave kinematics is closer to 1 at 12 s compared to 6s peak period.

Figure 14 also compares the dynamic responses of the lift wire tension with and without shielding effect when steady state simulation is applied. In this case, the dynamic responses are less influenced by the vessel shielding when compared with the transient case at 8 s peak period. The template maintains its position at the free water surface in steady state. As a result, the wave kinematics are not decaying and the template will experience more slamming loads, thus reducing the overall operational limits. However, the time history still shows an overall decrement in the lift wire tension with the shielding model.

The GEV distribution is used to fit the maximum tensions with and without shielding effect at different peak periods. A total of 100 maximum values of lift wire tension are generated from simulations using 100 wave seeds. The fitting of the probability density functions (PDF) of two wave conditions is compared in Figure 15. It can be observed the PDFs are significantly different with and without shielding at Tp = 6 s. The PDF of the

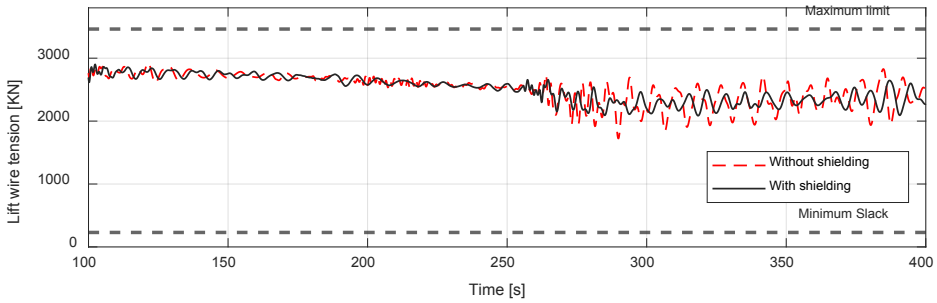

(a) Hs=1.8m, Tp=8s, Dir=165 deg

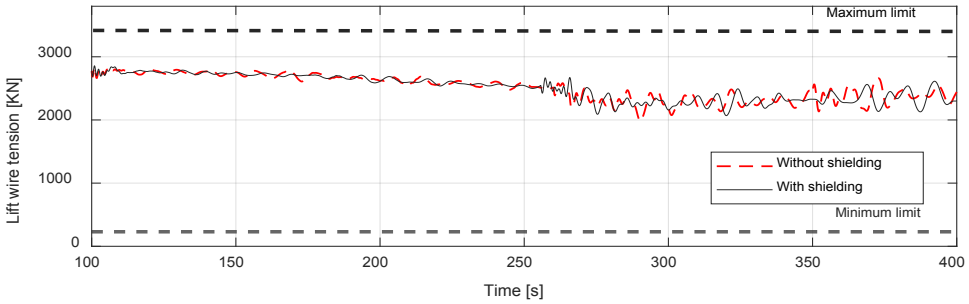

(b) Hs=1.8m, Tp=12s, Dir=165 deg

Figure 13. Time history of the lift wire tension with and without considering shielding effect at two Tp conditions.

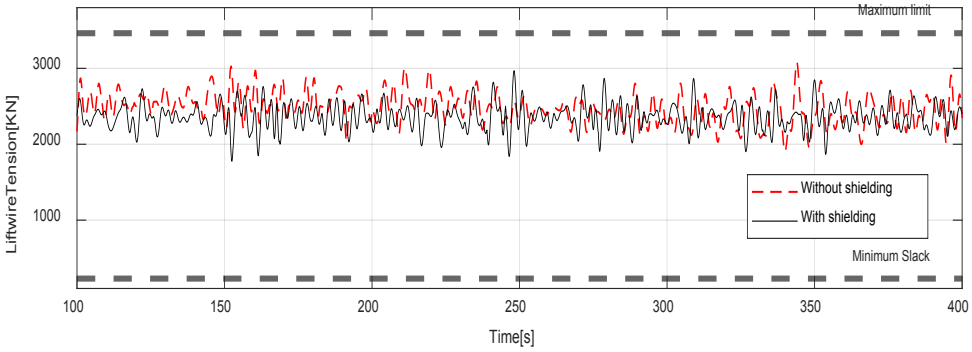

Figure 14. Comparing lift wire tension with and without shielding effect for using steady state approach (Hs=1.8, Tp=8 s, Dir=165 deg).

maximum tensions has more deviation from the mean value without the shielding effect. This is because the template is exposed to higher incident waves, which results in higher variability of the slamming forces using different wave realizations. As Tp increases to 12 s, the PDF of the maximum tensions is similar with and without the shielding effect.

6.2 Influence of the Wave Direction

The RAOs of the vessel and the shielding effect depend on the wave direction. In lifting operations, the vessel is often positioned heading to the incoming waves. At this position, the vessel will experience lower heave and roll motions compared to other headings. The heave, roll, and pitch motions dominate the crane tip responses as the lowering of the template takes place. The RAOs of the vessel's heave and roll for different wave directions are presented in Figure 16.

From Figure 16, the RAOs of both roll and heave motion are lowest when the wave direction is 180° across the given range of the wave peak period. As discussed earlier, the shielding effect is also sensitive to the wave direction. The installation vessel provides a shielding

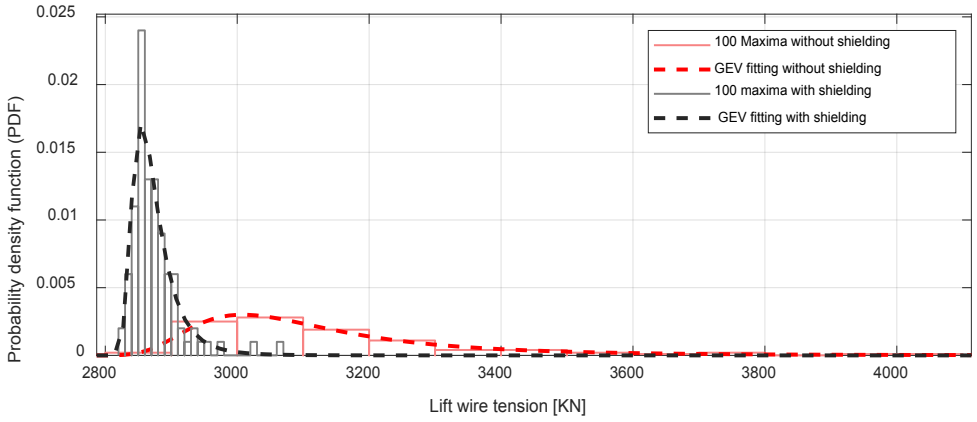

(a) PDF of the maxima at Tp = 6s, Hs = 2m

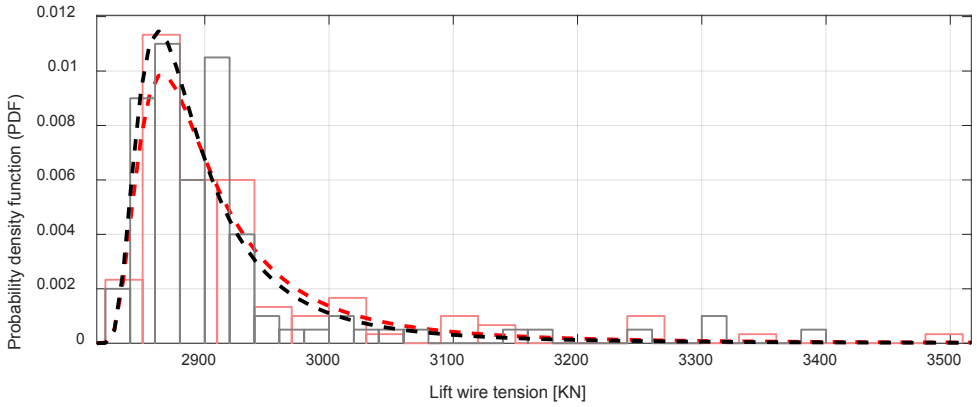

(b) PDF of the maxima at Tp = 12s, Hs = 2m

Figure 15. PDF functions of the maximum lift wire tensions with and without shielding effect.

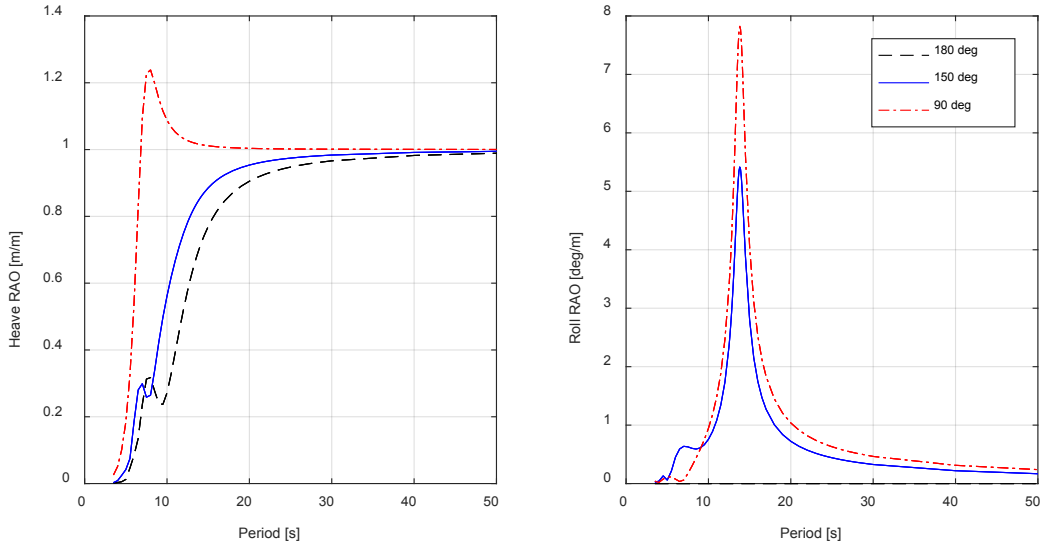

Figure 16. Heave and roll RAOs of the installation vessel.

effect for wave directions between 0° and 180 deg (See Figure 2). The disturbed wave kinematics RAO at 150 and 180 deg are also illustrated in Figure 7. The figure shows an increase in the wave RAO value when the wave direction is 180 deg compared to 150 deg. The influence of changing direction is more noticeable at Tp = 6 s with the RAO value increasing from 0.3 near the anchor location at 150 deg to almost 1 at 180 deg.

To further study the influence of wave directions on the responses of the dynamic system, simulations for three wave directions within a range of 150 to 180 deg using 50 seeds are performed. The chosen peak period is 8 s, and Hs is set to 2 m. 50 maxima of the lift wire tension are obtained from each seed for each wave direction. The maximum lift wire tensions under three wave directions are fitted using GEV distribution and compared in Figure 17. The lowest deviation from the mean tension value is obtained at 180 deg, while the highest is at 150 deg. Thus, it is concluded that a better shielding angle does not necessarily provide better operational limits since the vessel heave and roll RAOs have more influence on the lift wire maxima at any given wave direction.

6.3 Assessment of Allowable Sea State

The extreme value distributions introduced in Equations (7) and (8) are used as the statistical model for the lift wire extreme response. Although Gumbel distribution can provide a proper fitting for the extreme responses in various studies [6,18,27], this study aims to check the possibility of using the GEV distribution to achieve a better assessment of the allowable sea state based on the assigned target probability of non-exceedance. Figure 18 compares the probability plot fitting using the two mentioned distributions against the lift wire maxima. Both distributions show great variability when using different number of seeds. When 25 seeds are used, the plot shows poor fitting near the assigned target probability for both models. Applying the statistical model with this number of seeds can cause an underestimation of the extreme responses due to the outlier data at the tail. When 50 seeds are used, a better fitting is achieved at 0.95 probability of non-exceedance. Moreover, the overall deviation between GEV and Gumbel fittings is less compared to 25 seeds. At 100 seeds, the deviations between the two fittings start to be more obvious at lower probabilities. However, both distributions still provide a slightly more precise prediction of the extreme responses near the tail at 0.95 probability of non-exceedance.

From Figure 18 it can be concluded that assigning a target probability above 0.95 is not practical regardless of the number of seeds being used. The uncertainties of both statistical models are quite large for higher probabilities of non-exceedance. Furthermore, the study cannot conclude which statistical model provides a better fitting for the maxima since a perfect fitting at the tail is not achievable due to the outlier data.

In Figure 19, it is noticed that GEV provides an overall better fitting with the steady state approach for target probabilities below 0.95. However, at 0.95, both Gumbel and GEV provide an acceptable fitting for the maxima, especially when using 50 or 100 seeds. It is also noticed that assigning a target probability above 0.95 might be possible with GEV when 50 maxima or more are used with the steady state approach.

Since Figure 18 showed a slight variation when using 50 and 100 seeds compared to 25 seeds, the allowable sea states are evaluated based on 50 seeds for the maximum lift wire tension. Figure 20 compares the obtained allowable sea states using the GEV and Gumbel statistical models. The results are obtained using the transient approach

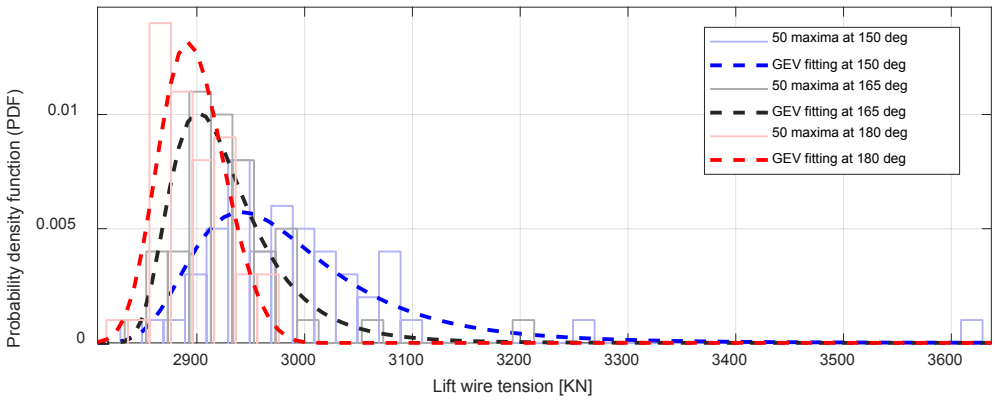

Figure 17. Lift wire maxima PDFs at three different wave directions (Hs = 2 m, Tp = 8 s).

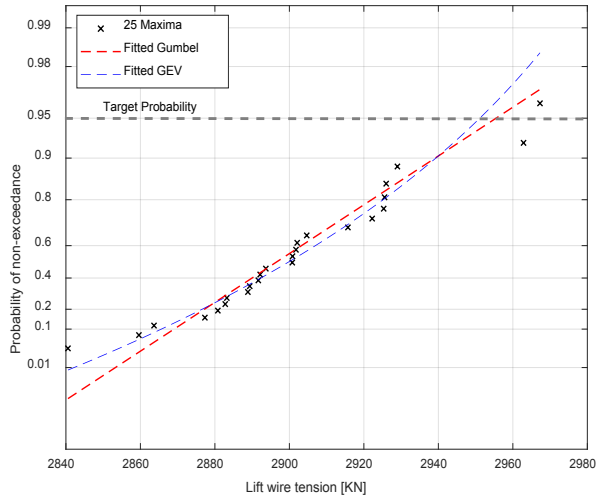

(a) 25 seeds

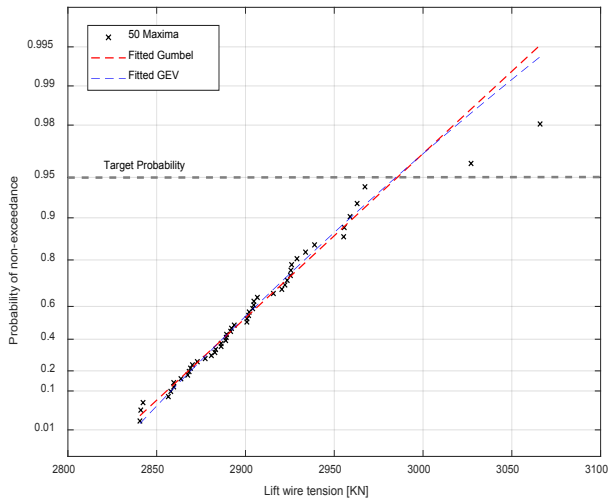

(b) 50 seeds

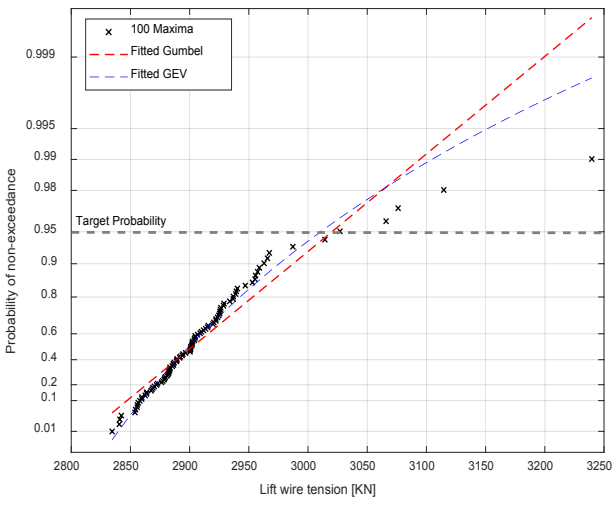

(c) 100 seeds

Figure 18. Probability paper plot for GEV and Gumbel distributions using transient approach with shielding (Hs =1.8 m, Tp =8 s, Dir =165 deg)

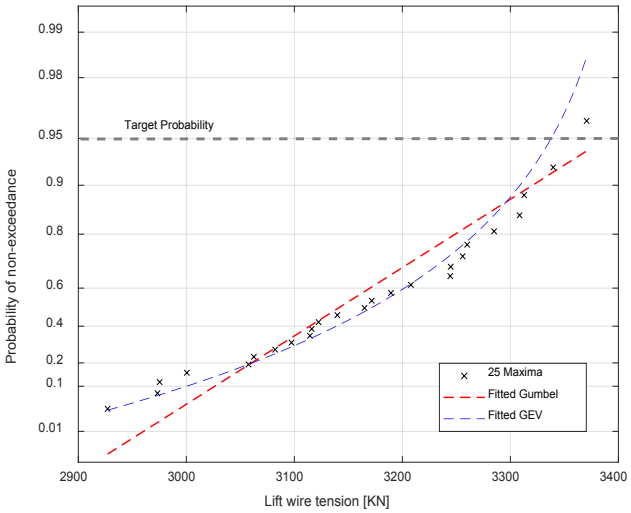

(a) 25 seeds

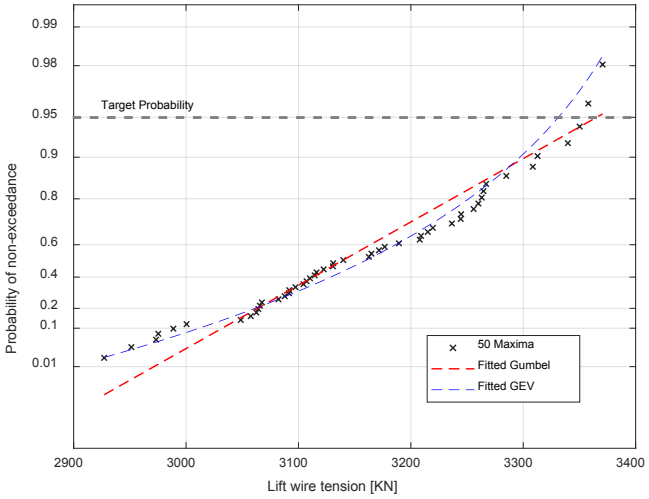

(b) 50 seeds

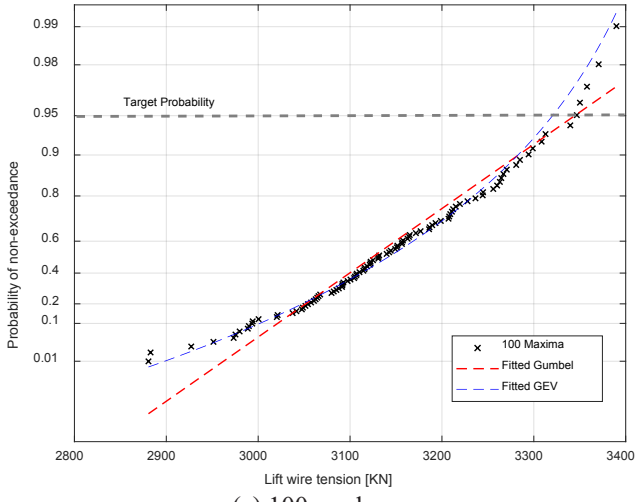

(c) 100 seeds

Figure 19. Probability paper plot for GEV and Gumbel distributions using steady state approach with shielding (Hs =1.8 m, Tp =8 s, Dir =165 deg)

with the shielding effect. The figure does not show any significant differences in the obtained sea states for both distributions. In general, the GEV result is slightly more conservative for the operational Hs across all the chosen Tp. Both distributions provide higher operational limits at lower Tp, especially when 180 deg wave direction is used.

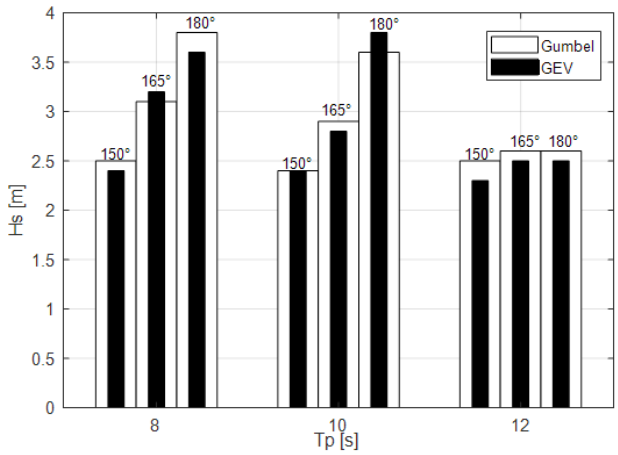

Figure 20. Comparing Gumbel and GEV using transient approach with shielding for different wave directions.

Table 8 compares the obtained allowable sea states for the operation based on GEV models. The comparison is carried out for three wave directions using transient and steady state approaches. The sea states are also compared with and without the shielding effect. A total of 50 lift wire maxima are used for the statistical model. When using transient approach, the allowable sea states are significantly higher at low peak periods with shielding effect, especially at 180 deg wave direction. This outcome is expected after the demonstrated results in Figure 15 and Figure 17.

In steady state, the shielding effect shows less influence on the limiting sea states compared to the transient approach. The template maintains its position at the free water surface in the steady state. As a result, the wave kinematics are not decaying and the template will experience more slamming loads, thus reducing the overall operational limits. Same as the transient approach, the highest operational Hs is obtained with shielding effect when the wave direction is 180 deg.

Based on this result, the steady state approach does not represent the real operational conditions, and the obtained allowable sea states using this approach will be over conservative, especially for short periods. Normally, the transient approach is more practical for similar studies when a sufficient number of seeds are used.

6.4 Influence of the Dimension of the Suction Anchor

The responses of the template and the lifting system during splash-zone crossing operation depend greatly on the slamming loads acting on the roof of the four suction anchors. Furthermore, Table 6 shows that the total added mass in both vertical and horizontal directions is almost 5 times larger than the actual mass of the whole template. Most of these inertia components are caused by the large size of the anchor. This reveals that the larger dimension of the suction anchors will cause higher slamming loads. To be more specific, when the diameter of the suction anchor increases, the volume of the trapped water inside the anchor will also increase, thus increasing the hydrodynamic added mass in the vertical direction. Larger diameters will also cause an increase in the drag forces on the anchor walls. To study the influence of the anchor size on the allowable sea states, three additional simulation cases are set up by changing the size of the template anchors. Hydrodynamic coefficients for each case are calculated accordingly while the same overall mass of the template is

Table 8. Allowable sea states using transient and steady state based on GEV statistical model.

		Hs[m] with shielding				Hs[m] without shielding		
Transient	Tp[s]\Dir[deg]	150	165	180	Tp[s]\Dir[deg]	150	165	180
	6	3.9	5 *	4.5*	6	1.7	2	2.1
	8	2.4	3.2	3.6	8	1.6	1.7	1.9
	10	2.4	2.8	3.8	10	1.9	2	2.2
	12	2.3	2.5	2.5	12	2.1	2.2	2.3
Steady state	Tp[s]\Dir[deg]	150	165	180	Tp[s]\Dir[deg]	150	165	180
	6	1.7	2.2	2.1	6	1.8	2	2.1
	8	1.9	2.2	2.3	8	1.7	1.9	2
	10	2.2	2.5	2.6	10	1.5	1.7	1.8
	12	2.3	2.4	2.6	12	1.5	1.6	1.7

* At Tp=6 s, the wave will break at such high Hs values. The wave breaking limit is not considered in this study.

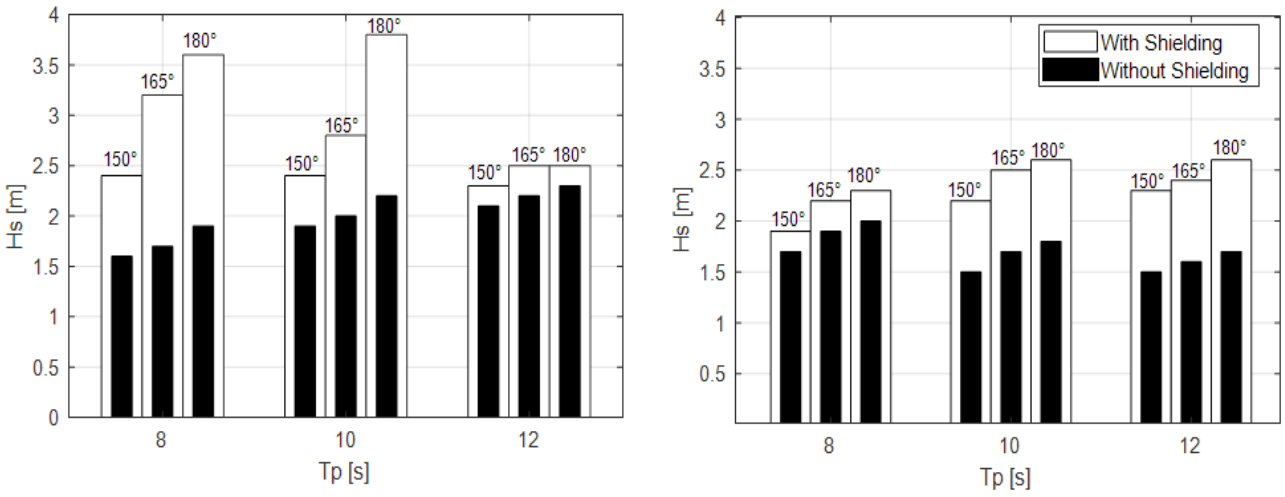

a) Transient approach

b) Steady State approach

Figure 21. Allowable sea states based on GEV statistical model

applied for all cases. Table 9 compares the hydrodynamic properties of the anchor from the original case with three new cases.

For each case, dynamic responses for 50 seeds are carried out at the same sea sate and wave direction, considering shielding effects. Figure 22 compares the GEV probability plot of the maxima lift wire tension for different cases. When the diameter is reduced to 4m (D4.0), the lift wire tension is 2885 KN at the target probability of non-exceedance. As the diameter increases, the tension increases gradually until it reaches 3160 KN at D5.5. Thus, it can be concluded that any change in the anchor diameter can alter the operational limits significantly. Smaller anchors are most likely to have higher allowable Hs for similar operations. Same as the previous results obtained in section 6.3, Figure 22 also shows that assigning a target probability higher than 0.95 for all cases is not practical when using 50 seeds. The GEV distribution shows an increased deviation in the fittings from actual values at higher probabilities. If a higher probability is assigned, the obtained lift wire tension from the statistical model can vary significantly from the actual value of the maxima.

The allowable sea states of the four cases with different anchor sizes are presented in Table 10 and Figure 23. From the table, it is seen that Case1 results in highest allowable Hs for all Tp conditions. The most noticeable outcome is when Tp is set to 8 s. The increment in Hs value is less significant when compared with other peak periods. This outcome is explainable through the eigenvalues analysis in Table 7. The analysis showed that the coupled system would experience higher dynamic responses around 8 s period. When the template is still above the water level,

Table 9. Anchor sizing hydrodynamic loads comparison.

Case name	Diameter [m]	Vertical added mass [ton]	Horizontal added mass [ton]	Vertical linear damping [kNs/m]	Horizontal quadratic damping [kNs^2/m^2]
Case1 (D4.0)	4	140	181	40	24
Case2 (D4.5)	4.5	183	225	44	27
Case3 (D5.0)	5	233	270	52	34
Original case (D5.5)	5.5	290	330	57	48

Table 10. Different anchor sizes allowable Hs using transient approach with shielding effect (wave direction 165 deg).

Case name	Tp [s]			
	6	8	10	12
Case1 (D4.0)	5.5 m	3.5 m	3.4 m	3.4 m
Case2 (D4.5)	5.4 m	3.4 m	3.3 m	3.2 m
Case3 (D5.0)	5.2 m	3.3 m	3 m	2.8 m
Original case (D5.5)	5 m	3.2 m	2.8 m	2.5 m

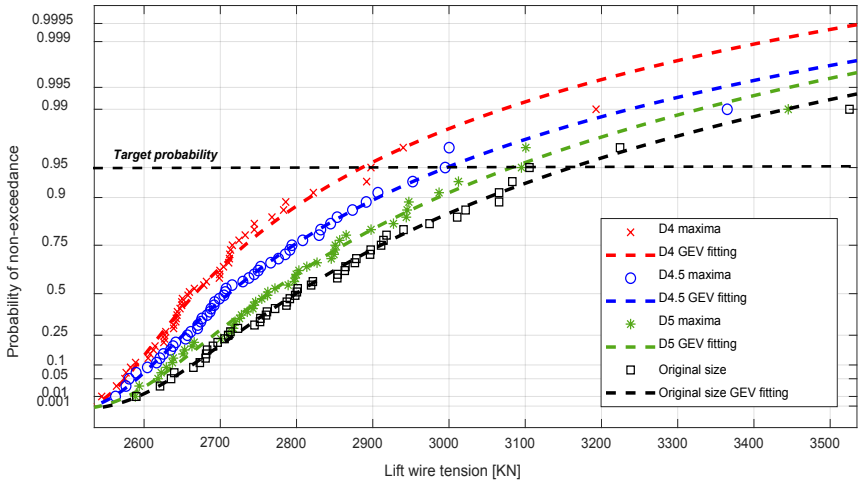

Figure 22. Non-linearized probability plot of the lift wire maxima for different anchor sizes. (Tp = 8 s, Hs = 3 m, Dir = 165 deg, with shielding)

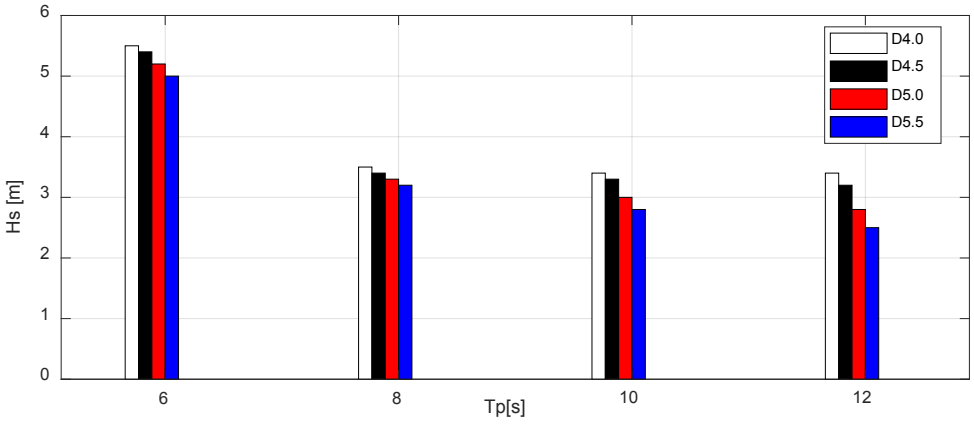

Figure 23. Different anchor sizes allowable Hs using transient approach with shielding effect (wave direction 165 deg).

the natural period is dominated by the vessel and the template pendulum motion. As the template reaches the free water surface, the vessel heave and roll motions start dominating the system at 8 s periods. These combined motions will accelerate the template body through the splash-zone, thus increasing the slamming loads according to Equation (2) and reducing the overall increment of Hs for smaller anchor diameters.

7. Conclusions

This paper presents a numerical study of splash-zone crossing operations for a subsea template. SIMA-SIMO is used to develop the fully coupled numerical model, which includes the installation bodies, the lifting system, and the hydrodynamic inputs. The hydrodynamic loads are calculated according to Morison's equation. Both frequency and time-domain simulations are performed to identify the critical response of the operation. The operation criteria are defined based on DNV guidelines and the operational sea states are evaluated.

Two time-domain simulation methods are used in the study, the transient and the steady state. The established numerical model is validated with actual field measurements before carrying out the allowable sea states assessment. Two statistical models (Gumbel, GEV) are employed in fitting the lift wire maxima to obtain the allowable sea states of the operation. The operational limits are assessed based on each model. The assessment is carried out for different wave directions and seeds number with and without shielding effect. The influence of changing the wave direction on both the vessel motion and the template is also discussed. Three cases with different anchor sizes are introduced to demonstrate the influence of

changing the anchor diameter on the slamming loads. The main findings are summarized as follows:

- The lift wire maximum tension is identified as the dominating limiting criterion for the operation. The most critical position for the template is defined when the anchors roof is at the splash-zone.
- In the transient approach, the vessel shielding shows more influence on improving the operational limits with short peak periods, especially when the waves are facing the vessel bow. However, the shielding has less influence when it comes to steady state simulations.
- The steady state approach does not represent the real operational conditions, and the obtained allowable sea states will be more conservative, especially for short periods. The transient approach is recommended for similar studies.
- The study showed big variability when using different number of seeds to establish the statistical model. It is also concluded that assigning a target probability of non-exceedance higher than 0.95 is not practical in this study due to the outlier data at the tail.
- It cannot be concluded whether Gumbel or GEV provides a better fitting for the extremes. Both distributions do not provide a perfect fitting, especially at the tails. In general, the differences between Gumbel and GEV are not big when used in obtaining the allowable sea states.
- Decreasing the anchor diameter can alter the operational limits significantly due to the decreased values of hydrodynamic drag and added mass. Thus, templates with the same total mass but smaller anchors are more likely to have higher operational limits at the same sea states.

Conflict of Interest

There is no conflict of interest.

References

[1] Li, Y., Zhao, H., Xu, N., et al., 2020. Study of the Installation Process of the Subsea Tree Passed Through the Splash Zone. Energies. 13(5), 1014.

[2] Jia, D., Agrawal, M., 2014. Fluid-structure interaction: lowering subsea structure/equipment in splash zone during installation. Offshore Technology Conference. Offshore Technology Conference.

[3] Wang, Y.Y., Tuo, H.H., Li, L.W., et al., 2018. Dynamic simulation of installation of the subsea cluster manifold by drilling pipe in deep water based on OrcaFlex. Journal of Petroleum Science and Engineering. 163, 67-78.

[4] Jacobsen, T., Naess, T.B., 2014. Installation of subsea structures using mid-size construction vessels in harsh environments. Offshore Technology Conference-Asia. Offshore Technology Conference.

[5] Gordon, R.B., Grytøyr, G., Dhaigude, M., 2013. Modeling suction pile lowering through the splash zone. ASME 2013 32nd International Conference on Ocean, Offshore and Arctic Engineering. American Society of Mechanical Engineers Digital Collection.

[6] Li, L., Parra, C., Zhu, X., et al., 2020. Splash zone lowering analysis of a large subsea spool piece. Marine Structures. 70, 102664.

[7] Li, L., Gao, Z., Moan, T., 2016. Operability analysis of monopile lowering operation using different numerical approaches. ISOPE.

[8] DNV·GL, 2017. Recommended practice: Modelling and analysis of marine operations, DNVGLRP-N103.

[9] DNV·GL, 2017. Recommended practice: Lifting appliances used in subsea operations, DNVGL-RP-N201.

[10] Acero, W.G., Li, L., Gao, Z., et al., 2016. Methodology for assessment of the operational limits and operability of marine operations. Ocean Engineering. 125, 308-327.

[11] Li, L., Gao, Z., Moan, T., 2015. Response Analysis of a Nonstationary Lowering Operation for an Offshore Wind Turbine Monopile Substructure. Journal of Offshore Mechanics and Arctic Engineering. 137(5).

[12] Bai, Y., Bai, Q., 2010. Subsea engineering handbook. Elsevier: Amsterdam; Boston; Paris.

[13] Bunnik, T., Buchner, B., 2004. Numerical prediction of wave loads on subsea structures in the splash zone. in The Fourteenth International Offshore and Polar Engineering Conference. International Society of Offshore and Polar Engineers.

[14] Damblans, G., Berhault, C., Marcer, R., et al., 2012. CFD and Experimental Investigations of Slamming Load Prediction on Subsea Structures in Splash Zone. The Twenty-second International Offshore and Polar Engineering Conference. OnePetro.

[15] Buchner, B., Bunnik, T., Honig, D., et al., 2003. A new simulation method for the installation of subsea structures from the splash zone to the ultra deep. DOT conference

[16] Ren, B., Wang, Y., 2004. Numerical simulation of random wave slamming on structures in the splash zone. Ocean Engineering. 31(5-6), 547-560.

[17] DNV·GL, 2014. Loadout, transport and installation of subsea objects, DNVGL-OS-H206.

[18] Li, L., Amer, A.M., Zhu, X., 2020. Numerical analysis of an over-boarding operation for a subsea template. Journal of Ocean Engineering and Science.

[19] Ocean, S., 2018. SINTEF Ocean, SIMO 4.12.1 Theory Manual.

[20] DNV·GL, 2018. Enviromental conditions and environmental loads, DNVGL-RP-C205.

[21] Solaas, F., Sandvik, P.C., 2017. Hydrodynamic coefficients for suction anchors during installation operations. in ASME 2017 36th International Conference on Ocean, Offshore and Arctic Engineering. American Society of Mechanical Engineers Digital Collection.

[22] Li, L., Gao, Z., Moan, T., 2015. Comparative study of lifting operations of offshore wind turbine monopile and jacket substructures considering vessel shielding effects. The Twenty-fifth International Ocean and Polar Engineering Conference. OnePetro.

[23] Li, L., Zhen, G., Moan, T., et al., 2014. Analysis of lifting operation of a monopile for an offshore wind turbine considering vessel shielding effects. Marine Structures. 39, 287-314.

[24] Næss, T., Havn, J., Solaas, F., 2014. On the importance of slamming during installation of structures with large suction anchors. Ocean Engineering. 89, 99-112.

[25] DNV·GL, 2016. Standard: Marine operations and marine warranty, DNVGL-ST-N001.

[26] Baarholm, G.S., Haver, S., Økland, O.D., 2010. Combining contours of significant wave height and peak period with platform response distributions for predicting design response. Marine Structures. 23(2), 147-163.

[27] Solaas, F., Sandvik, P.C., Pâkozdi, C., et al., 2017. Dynamic forces and limiting sea states for installation of grp protection covers. International Conference on Offshore Mechanics and Arctic Engineering. American Society of Mechanical Engineers.